

基于新型光子晶体光纤近红外波段的传感特性

张文^{1,2}, 白冰冰^{1,2}, 张砚曾^{1,2}, 陈聪^{1,2}, 邵齐元^{1,2}, 陈灿灿^{1,2}, 王浩然^{1,2}, 刘海^{1,2*}¹中国矿业大学地下空间智能控制教育部工程研究中心, 江苏 徐州 221116;²中国矿业大学信息与控制工程学院, 江苏 徐州 221116

摘要 利用有限元方法研究了八边形包层结构的光子晶体光纤的光学特性,并结合填充技术具体分析了光流体折射率对数值孔径、有效模场面积等参数的影响。通过在直波导中填充光学流体,可明显降低限制损耗,且在波长 $1.56 \mu\text{m}$ 处的限制损耗为 $0.00172 \text{ dB} \cdot \text{m}^{-1}$,色散参数为 $0.00018 \text{ ps} \cdot \text{THz}^{-1} \cdot \text{cm}^{-2}$,相对灵敏度达 66%。该八边形包层结构在宽波长范围内能够实现低色散的光信号传输,同时为高灵敏度的气体传感检测提供了新方案。

关键词 光子晶体; 相对灵敏度; 色散; 气体检测

中图分类号 TN25

文献标志码 A

doi: 10.3788/CJL202148.0706001

1 引言

光子晶体光纤(PCF)因其独特的控光特性,在气体传感^[1]、全光开关^[2]、四波混频^[3]等领域得到广泛的应用。近年来,随着损耗和成本的降低,基于PCF设计的传感器具有吸收路径短、检测灵敏等特点,成为研究人员的关注热点^[4-6]。2014年,Ademgil^[7]研究了八边形光子晶体光纤结构的传输特性,该结构相较于传统六边形包层结构具有更高的相对灵敏度。2015年,Ademgil等^[8]提出了一种椭圆形包层PCF结构,结合液体渗透技术分析得到该结构具有较高的相对灵敏度(23.45%)和较低的限制损耗($5.5 \times 10^{-5} \text{ cm}^{-1}$)。2016年,Asaduzzaman等^[9]通过对纤芯和包层进行优化,设计了一种用于化学传感的混合PCF结构,该结构对苯、乙醇的相对灵敏度分别为48.85%和49.17%。2018年,Sultana等^[10]设计了一种可用于太赫兹频率范围感测的PCF结构,通过在纤芯位置引入多孔区域来限制纤芯能量,实现高双折射。同年,廖昆等^[11]证明了基于椭圆空气孔的缺陷型PCF结构具有高双折射。2019年,Sardar等^[12]基于PCF分析了混合多孔芯的中红外范围的光学特性,通过对结构参数的优化实现了21.2%的相对灵敏度,该研究

为气体检测提供了新的思路。同年,廉正刚等^[13]分析了微结构光纤的导光机理及其在传感领域的应用,该研究为后续研究提供了理论基础。2020年,丛海芳等^[14]通过选择空芯带隙型光子晶体光纤(单端镀全反膜)作为光学气室,实现了置入式同源甲烷浓度的探测。然而,众多学者仅对灵敏度、限制损耗等光学参数进行了优化,忽略了色散效应对光信号的影响,色散过大时极有可能会造成光脉冲被展宽,使得相邻的脉冲出现重叠,从而使得误码率增大,这将不利于光的传播,因此如何减小色散并提高检测灵敏度是一个挑战。

本文研究了具有多槽波导的八边形PCF结构,通过参数优化获得最佳结构,并通过在靠近纤芯的两个槽中填充光学流体来研究光流体技术对光学特性的影响。其中色散参数的范围为 $(0.041 \pm 0.023) \text{ ps} \cdot \text{THz}^{-1} \cdot \text{m}^{-2}$,相对灵敏度达65%以上。所提结构为有害气体的精准检测提供了可能,同时在近红外波长范围内实现了光信号低色散、近于平坦的高效传输。

2 理论模型优化与传感原理

基于八边形PCF结构的截面示意图如图1(a)所示,晶格常数 $a=3 \text{ m}$,光纤的包层为八边形空气孔结

收稿日期: 2020-08-20; 修回日期: 2020-08-28; 录用日期: 2020-10-14

基金项目: 国家自然科学基金(51874301)、徐州市重点研发项目(KC20162)

*E-mail: Lhai_hust@hotmail.com

构,其空气孔的直径 $d=0.7a$,基底为二氧化硅,其折射率为 1.45。由于在圆形气孔中很难保持极化状态,因此在纤芯区域设置对称的直波导来保持偏振态,同时利用矩形结构来增强 PCF 结构的双折射。图 1(b)

和(c)给出了波长位于 1550 nm 处 X 偏振方向和 Y 偏振方向的电场能量图,从图 1 中可以看出,光主要分布在纤芯区域,这种模式被称为纤芯基模。为了准确分析相关结果,选取该模式来研究光学特性。

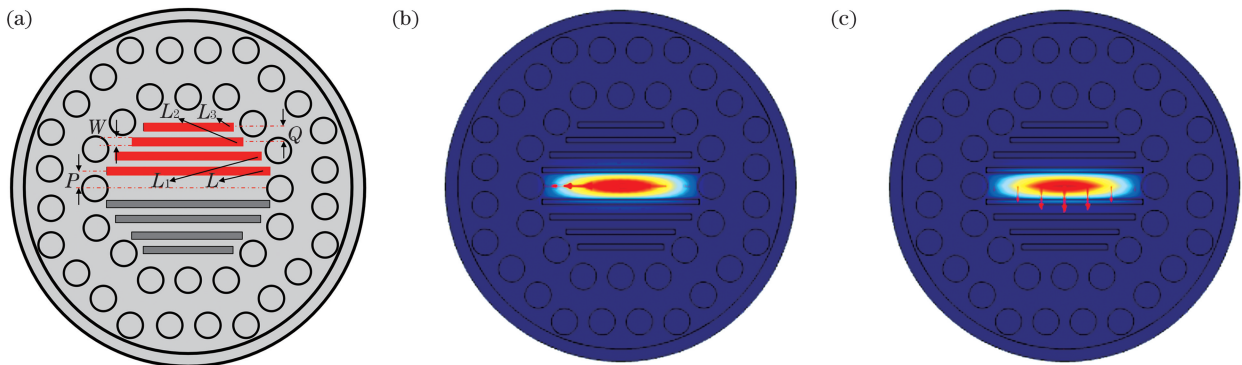


图 1 光子晶体光纤结构的截面示意图和纤芯基模能量分布图。(a) 基于八边形包层结构的 PCF 结构图;(b) X 偏振方向的能量分布;(c) Y 偏振方向的能量分布

Fig. 1 Cross-sectional view of PCF structure and energy distributions of fundamental mode of fiber core. (a) PCF structural diagram based on octagonal cladding structure; (b) energy distribution in X polarization direction; (c) energy distribution in Y polarization direction

限制损耗是衡量光纤传感特性的一个重要参数^[15]。采用有限元法(FEM)可获得模式的有效折射率 n_{eff} ,然而由于包层空气孔的数量是有限的,因此不可避免地会产生光的泄漏,泄漏到材料中的光会导致限制损耗,限制损耗 L_c 可表示为

$$L_c = \frac{20}{\ln 10} \times \frac{2\pi}{\lambda} \times \text{Im}(n_{eff}), \quad (1)$$

式中: λ 为真空中的波长; $\text{Im}(n_{eff})$ 为模式有效折射率的虚部。首先探讨包层气孔直径对限制损耗的影响,图 2 反映了光纤的限制损耗 L_c 随波长的变化。如图 2 所示,随着气孔直径的增大,限制损耗减小,

这是由于空气孔的尺寸增大限制了光的泄漏,从而使得损耗减小。同时限制损耗随波长的增加而增大,这是因为随着波长的增大,包层和纤芯的折射率差减小,从而使得光信号泄漏到包层中。

如图 1(a)所示,将矩形波导的宽度定义为 $W=0.15a$,两个波导的间距定义为 $Q=0.35a$,波导的长度 L, L_1, L_2, L_3 分别为 $4.2a, 3.8a, 2.9a, 2.3a$ 。讨论第一个直波导与纤芯的距离 P 对相对灵敏度的影响。图 3 表明了纤芯直波导的位置变化对相对灵敏度的影响,随着纤芯直波导远离 L_1 ,相对灵敏度变小, $P=0.35a$ 和 $P=0.40a$ 时的相对灵敏度较

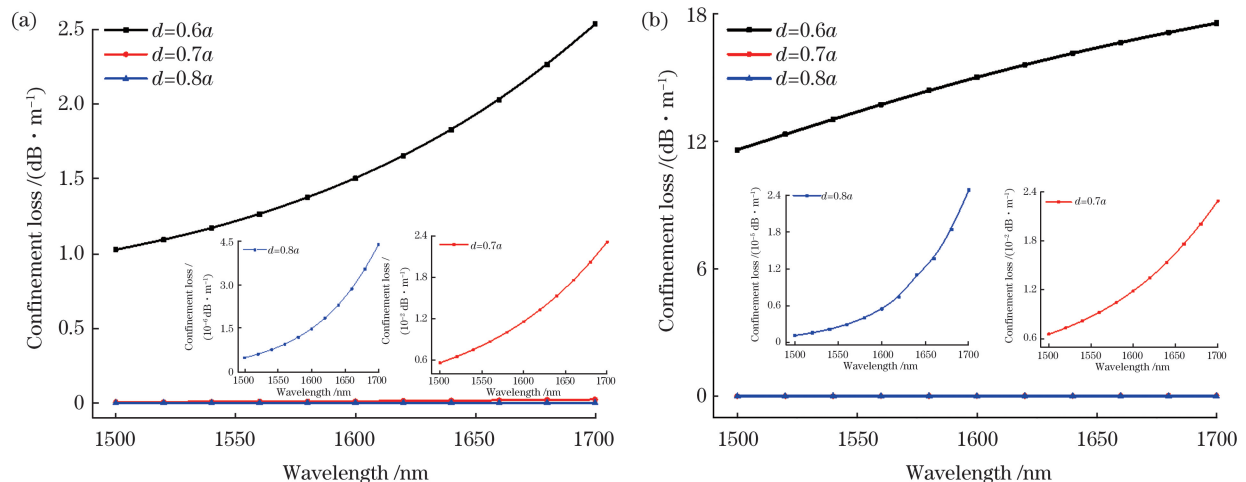


图 2 不同偏振方向的限制损耗与波长的变化关系。(a) X 偏振;(b) Y 偏振

Fig. 2 Relationship between confinement loss and wavelength in different polarization directions. (a) X polarization direction; (b) Y polarization direction

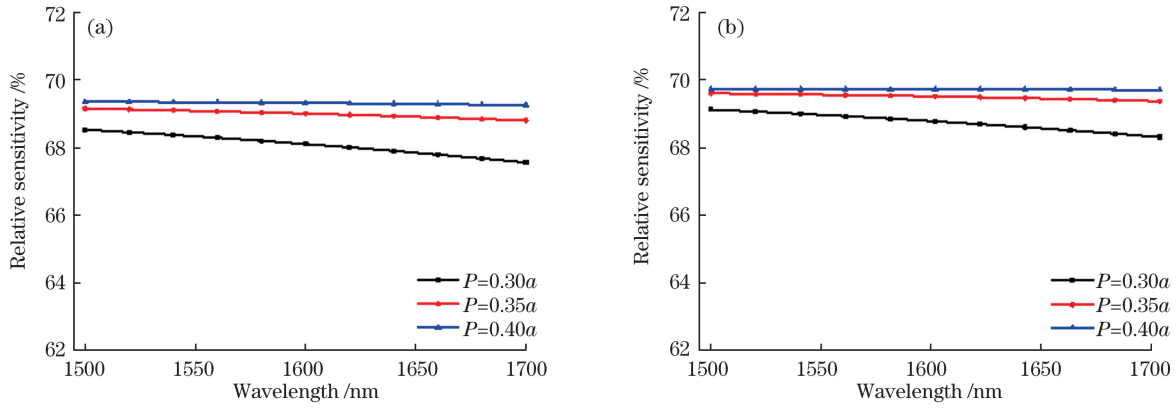


图 3 纤芯直波导位置变化对相对灵敏度的影响。(a) X 偏振方向;(b) Y 偏振方向

Fig. 3 Influence of position change of fiber core straight waveguide on relative sensitivity. (a) X polarization direction; (b) Y polarization direction

接近,均在 69%左右,考虑到制造效率,在后续研究中 P 取 0.35a。

在各种气体的红外光谱中,吸收带的独特性对于气体的痕量具有重要意义^[16-18]。当一束强度为 I_0 的光通过光子晶体光纤时,待测气体对光场具有吸收作用,使得通过待测气体的光的强度发生变化,输出光强 I 满足朗伯-比尔定律^[19-20],即

$$I(\lambda) = I_0(\lambda) \exp[-r\alpha(\nu)Cd], \quad (2)$$

式中: ν 为光波长 λ 处的速度; α 为待测气体分子在光波长 λ 处的吸收系数 (cm^{-1}); d 为穿过吸收介质的光的相互作用的路径长度 (cm); r 为相对灵敏度; C 为吸收材料的浓度。

待测样品的吸光度为

$$A = \lg\left(\frac{I}{I_0}\right) = -r\alpha(\nu)Cd, \quad (3)$$

其中浓度 C 可表示为

$$C = \frac{1}{-r\alpha(\nu)d} \lg\left(\frac{I}{I_0}\right). \quad (4)$$

通常在光纤中用相对灵敏度 r 来描述光与物质的相互作用,其中 r 与填充物的折射率 n 、导模的有效折射率 n_{eff} 以及功率分布函数 e 的关系为

$$r = \frac{n_r}{n_{\text{eff}}} \times e. \quad (5)$$

根据坡印廷定理,功率分布函数 e 、 f 可由电场 E 和磁场 H 求得,即

$$e = \frac{\int_{\text{sample}} R_e(E_x H_y - E_y H_x) dx dy}{\int_{\text{total}} R_e(E_x H_y - E_y H_x) dx dy} \times 100\%$$

$$f = \frac{\int_{\text{sample}} R_e(E_x H_y - E_y H_x) dx dy}{\int_{\text{total}} R_e(E_x H_y - E_y H_x) dx dy} \times 100\%, \quad (6)$$

式中: R_e 为 $E \times H$ 的实部; E_x 和 H_x 分别为 x 方向的电场和磁场; E_y 和 H_y 分别为 y 方向的电场和磁场。 R_e 越大,表明光与物质的相互作用越强,气体的吸收能力越强,因此相对灵敏度会变大,这对传感检测更有利。

图 4(a)、(b)为不同极化方向的相对灵敏度,随着空气孔尺寸的增大,相对灵敏度减小,在相同 d 下,Y 方向灵敏度高于 X 方向,且两个方向的灵敏度均在 60%以上,这对传感是极为有利的。图 4(c)、(d)为不同极化方向的基模的有效折射率,随着波长的增加,有效折射率减小,气孔直径的变化对有效折射率的影响较小。

由光强相互作用所覆盖的面积可以用有效模场面积来计算。一个较大的模态有效面积适用于激光和通信设备,而较小的模态有效面积适用于非线性效应,可表示为

$$A_{\text{eff}} = \frac{\left[\iint |E(x, y)|^2 dx dy \right]^2}{\iint |E(x, y)|^4 dx dy}, \quad (7)$$

式中: $E(x, y)$ 为电场分布,求解域选择光纤的纤芯截面。

数值孔径 (NA) 越大,对传感应用越有利。当 PCF 的纤芯和包层之间的折射率差越大时,数值孔径 (NA) 越接近 1。NA 可量化为

$$NA = \frac{1}{\sqrt{1 + \frac{\pi A_{\text{eff}} f^2}{c^2}}}, \quad (8)$$

式中: f 为频率。

图 5(a)显示了有效模场面积 A_{eff} 随波长的变化关系。随着孔径尺寸的增大,模场面积增大,而数值孔径逐渐减小,这与(8)式是一致的。由于 NA

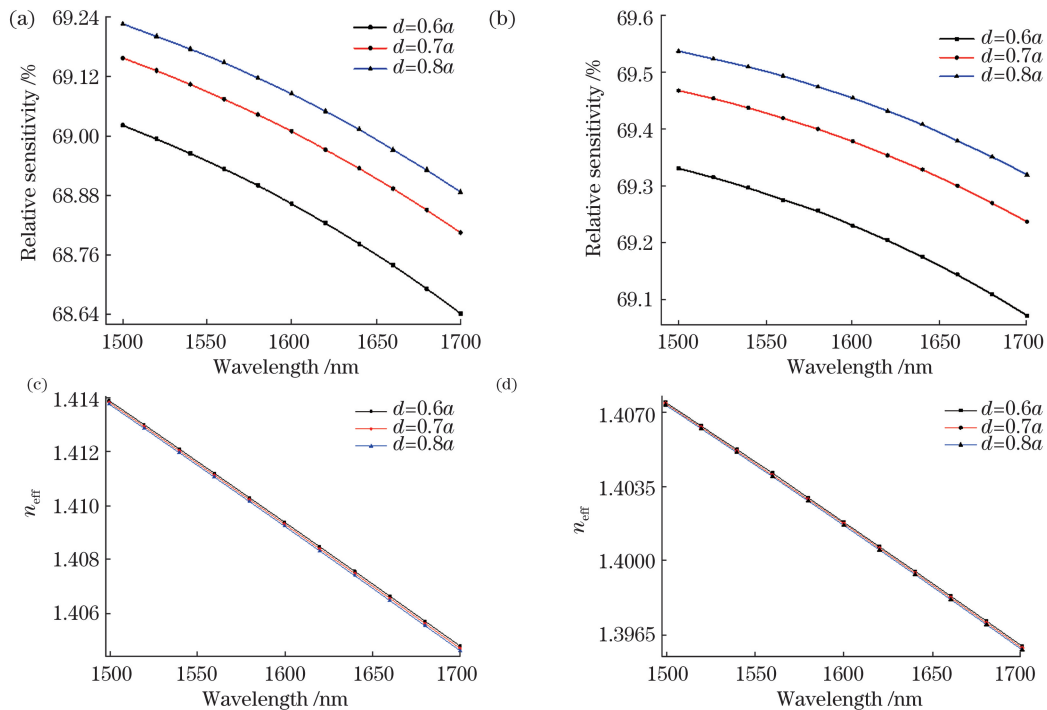


图 4 不同参数条件下基模的相对灵敏度和有效折射率随波长的变化关系。(a) X 偏振方向的相对灵敏度;(b) Y 偏振方向的相对灵敏度;(c) X 偏振方向的有效折射率;(d) Y 偏振方向的有效折射率

Fig. 4 Relationship between relative sensitivity and effective refractive index of fundamental mode with wavelength under different parameters. (a) Relative sensitivity in X polarization direction; (b) relative sensitivity in Y polarization direction; (c) effective refractive index in X polarization direction; (d) effective refractive index in Y polarization direction

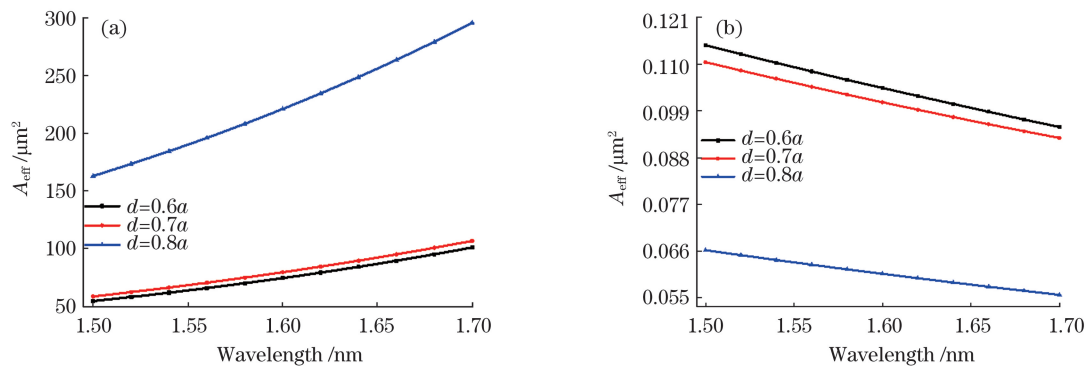


图 5 不同孔径尺寸的模场面积 A_{eff} 、数值孔径 NA 与波长的关系。(a)模场面积 A_{eff} ;(b)数值孔径 NA

Fig. 5 Relationship among mode field area A_{eff} , numerical aperture NA, and wavelength for different aperture sizes.

(a) Mode field area A_{eff} ; (b) numerical aperture NA

越理想,越有利于传感检测,因此考虑 L_c 、 r 、 NA ,确定最佳的结构为 $d=0.7a$ 。在最佳设计参数下, NA 为 0.11[图 5(b)]。

3 数值结果与分析

随着光流体的出现,从微观尺度上操纵光路和流体来改变介质的光学能力,已经成为制造高灵敏传感器的重要手段。通过改变折射率 n 调整光子电路的光学特性,可使光子设备具有可调性和可重构

性,使其可用于气体传感检测^[21]。如图 6 所示,使用准直镜、聚焦镜等光学器件将两根单模光纤(SMF)和 PCF 连接,并利用显微镜和飞秒激光技术在 PCF 的连接端面钻出两个微孔,以实现气体的精准填充^[22-23]。

通过在靠近纤芯两侧的直波导处填充光学流体,来探究其折射率 n_1 对 PCF 各光学参数的影响,为了确保光学流体仅进入纤芯而不进入包层气孔,可通过皮下注射针等细小尖端设备,将光学流体缓

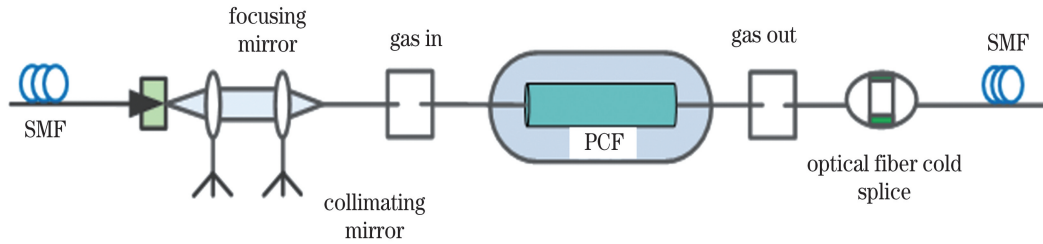


图 6 光子晶体光纤气体传感原理图

Fig. 6 Principle diagram of photonic crystal fiber gas sensing

慢注入光纤或在光纤的一端沉积一层包层来阻止光学流体的进入。设置未填充的光学流体的折射率为 1.0 以及填充的折射率分别为 1.1、1.2, 如图 7 所示, 随着波长的增加, 限制损耗变大, 这是由于在较大的波长处, 纤芯和包层间的相对折射率的降低使

得更多的光信号泄漏到包层中。在图 7(a) 中, 限制损耗随着填充光流体折射率 n_1 的增加而减小, L_c 的数量级在 10^{-2} , 而在图 7(b) 中, L_c 随着 n_1 的增加先增加后减小, 相同 n_1 时 Y 偏振方向比 X 偏振方向的限制损耗高两个数量级。

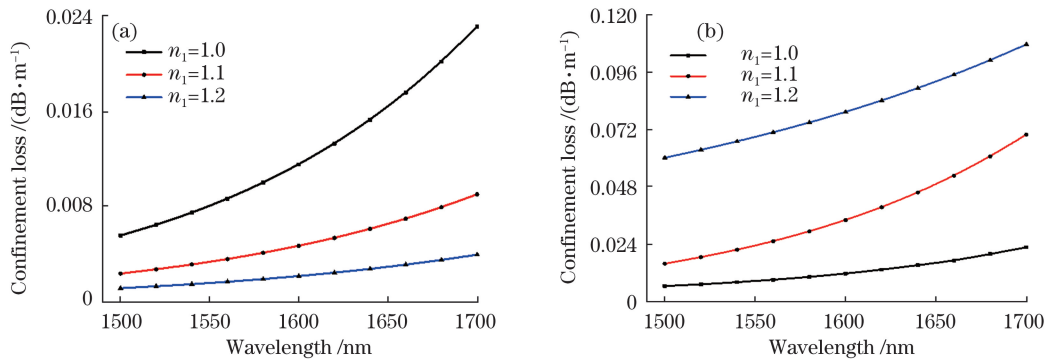


图 7 不同光流体折射率下的限制损耗随波长的变化关系。(a) X 偏振方向的限制损耗; (b) Y 偏振方向的限制损耗

Fig. 7 Relationship between confinement loss and wavelength under different optical fluid refractive indexes.

(a) Confinement loss in X polarization direction; (b) confinement loss in Y polarization direction

图 8 显示了不同光流体折射率下的相对灵敏度, 不论是 X 偏振方向还是 Y 偏振方向, 相对灵敏度都随着填充光流体折射率的增加呈减小趋势, 且随着波长的增加而减小。相比于 X 偏振方向, 相同结构条件下的 Y 偏振方向的灵敏度较高, 且该模型的相对灵敏度均在 65% 以上, 这对于传感检测是极

为有利的。

图 9 表明了不同 n_1 下的有效折射率 n_{eff} 与波长之间的关系, 随着波长的增加, n_{eff} 呈现递减的趋势, 这是由于在较大的波长处, 光的传播速度较大, 相应的折射率较低。填充光学流体使得有效折射率增大, 因此 n_{eff} 曲线相较于未填充的结构明显上移。

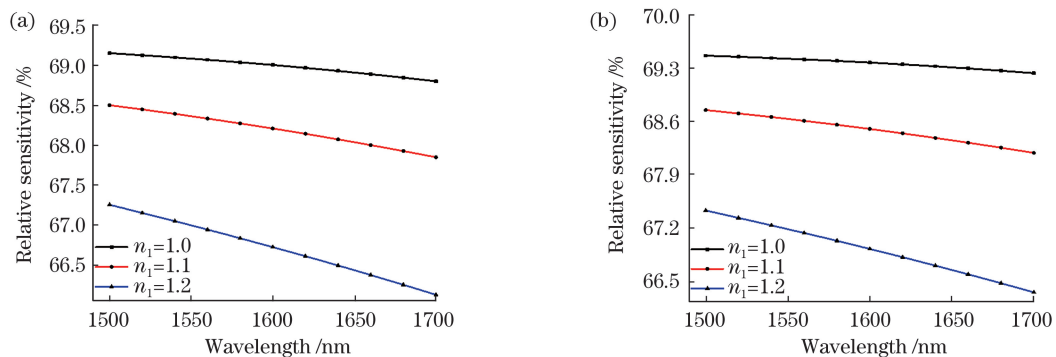


图 8 不同光流体折射率下的相对灵敏度随波长的变化。(a) X 偏振方向的相对灵敏度; (b) Y 偏振方向的相对灵敏度

Fig. 8 Relationship between relative sensitivity and wavelength under different optical fluid refractive indexes. (a) Relative sensitivity in X polarization direction; (b) relative sensitivity in Y polarization direction

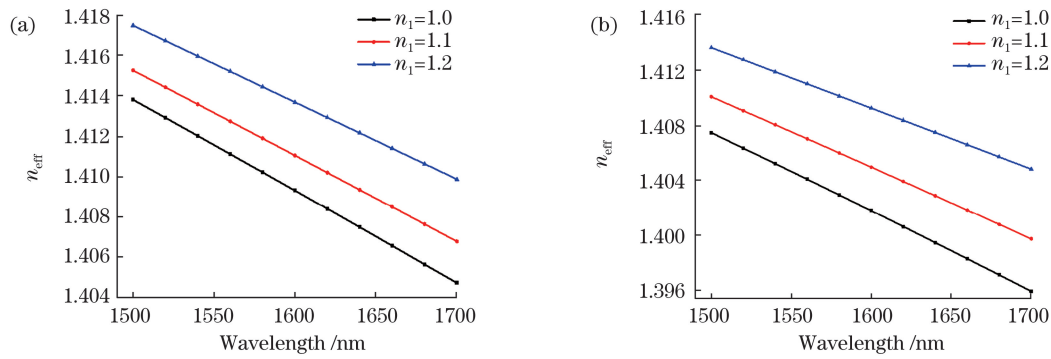


图 9 不同偏振方向的有效折射率和波长的关系。(a) X 偏振方向;(b) Y 偏振方向

Fig. 9 Relationship between effective refractive index and wavelength in different polarization directions.

(a) X polarization direction; (b) Y polarization direction

图 10 显示了不同 n_1 下的模场面积 A_{eff} 、数值孔径 NA 与波长之间的关系,随着波长的增加, A_{eff} 呈现递增的趋势, NA 呈现递减的趋势。填充光学

流体使得有效折射率增加,因此 A_{eff} 相较于未填充的结构明显上移, NA 相较于未填充的结构发生下移但变化较小。

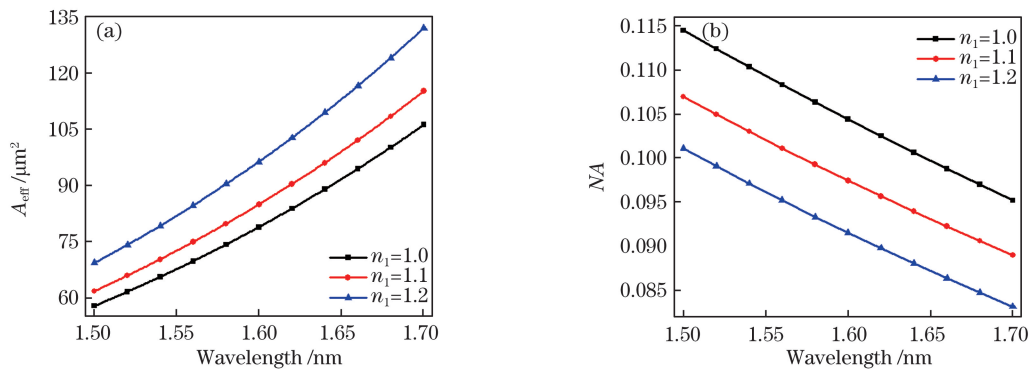


图 10 不同填充折射率下的模场面积 A_{eff} 和数值孔径 NA 。(a) A_{eff} ;(b) NA

Fig. 10 Mode field area A_{eff} and numerical aperture NA under different filling refractive indexes. (a) A_{eff} ; (b) NA

PCF 的特性不仅与填充有关,还与包层空气孔的大小和形状有关,通过调节 PCF 的结构可实现低损耗、高相对灵敏度的光传输。此外,使用不同的流体材料实现光对物质的控制,通过在光纤的气孔中引入光流体技术对模式进行动态调节,这降低了因更换光纤产生的成本,有利于高灵敏度的集成传感器的构建。

在实际的应用中,需要考虑光纤对多通道通信应用的操作能力,即色散。由于材料色散可忽略不计,因此仅需计算所提出的 PCF 的波导色散。光纤的波导色散参数 β (单位为 $\text{ps} \cdot \text{THz}^{-1} \cdot \text{cm}^{-2}$)为

$$\beta = \frac{2}{c} \frac{dn_{\text{eff}}}{d\omega} + \frac{\omega}{c} \frac{d^2 n_{\text{eff}}}{d\omega^2}, \quad (9)$$

式中: ω 为角频率。

图 11 表明不同光流体折射率(n_f)下波长的色散特性,在 $1.55 \sim 1.64 \mu\text{m}$ 范围内获得的色散范围为 $(0.041 \pm 0.023) \text{ps} \cdot \text{THz}^{-1} \cdot \text{cm}^{-2}$,相对于之前

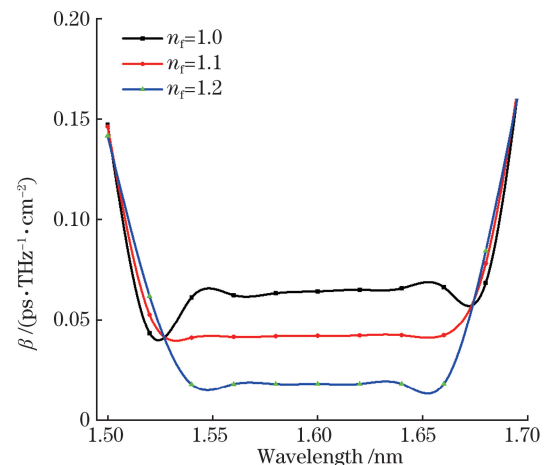


图 11 不同光流体折射率下色散与波长的关系

Fig. 11 Relationship between dispersion and wavelength at different refractive indexes of light fluid

提出的结构^[24-26],所提结构的色散非常低且平坦度得到显著改善,如表 1 所示。

表 1 各结构的参数比较

Table 1 Comparison of parameters of each structure

Type of structure	Frequency or wavelength	$r / \%$	$L_c / (\text{dB} \cdot \text{m}^{-1})$	$\beta / (\text{ps} \cdot \text{THz}^{-1} \cdot \text{cm}^{-2})$
Structure in Ref. [12]	3 THz	30.0	0.01	0.35
Structure in Ref. [14]	3 THz	60.0	0.01	0.52
Structure in Ref. [15]	1 THz	84.0	0.00295	0.63
Structure in Ref. [9]	1 THz	50.0	8.656×10^{-11}	0.07
Proposed structure	1.56 μm	66.9	0.00172	0.00018

4 结 论

设计了一种新型 PCF, 采用有限元方法研究了近红外范围内的光学特性, 并利用优化的结构和光流体技术分析了填充光流体对相对灵敏度、限制损耗、色散参数的影响。结果表明所设计结构在 1.55~1.64 μm 的波长范围内具有明显的接近零的平坦色散特性, 相对灵敏度在 65% 以上。在较宽的近红外波长范围内通过填充光流体实现了 $1.52 \times 10^{-2} \sim 2.8 \times 10^{-2} \text{ dB} \cdot \text{m}^{-1}$ 低损耗和 $0.018 \text{ ps} \cdot \text{THz}^{-1} \cdot \text{cm}^{-2}$ 超低色散的光信号传播。此外, 由于结构具有灵活性, 通过调节结构参数有望实现 THz 范围内的气体传感检测。

参 考 文 献

- [1] Anas M T, Asaduzzaman S, Ahmed K, et al. Investigation of highly birefringent and highly nonlinear Hexa Sectored PCF with low confinement loss[J]. Results in Physics, 2018, 11: 1039-1043.
- [2] Badran H A, Abul-Hail R C, Shaker H S, et al. An all-optical switch and third-order optical nonlinearity of 3, 4-pyridinediamine [J]. Applied Physics B, 2016, 123(1): 31.
- [3] Geng Y F, Wang L N, Tan X L, et al. A compact four-wave mixing-based temperature fiber sensor with partially filled photonic crystal fiber [J]. IEEE Sensors Journal, 2019, 19(8): 2956-2961.
- [4] Wang F, Sun Z, Liu C, et al. A high-sensitivity photonic crystal fiber (PCF) based on the surface plasmon resonance (SPR) biosensor for detection of density alteration in non-physiological cells (DANCE) [J]. Opto-Electronics Review, 2018, 26(1): 50-56.
- [5] Arif M F H, Biddut M J H. Enhancement of relative sensitivity of photonic crystal fiber with high birefringence and low confinement loss [J]. Optik, 2017, 131: 697-704.
- [6] Sardar M R, Faisal M. Gas sensor based on octagonal hollow core photonic crystal Fiber [C] // 2017 IEEE International Conference on Imaging, Vision & Pattern Recognition (icIVPR), February 13-14, 2017, Dhaka, Bangladesh. New York: IEEE Press, 2017: 1-4.
- [7] Ademgil H. Highly sensitive octagonal photonic crystal fiber based sensor [J]. Optik, 2014, 125 (20): 6274-6278.
- [8] Ademgil H, Haxha S. PCF based sensor with high sensitivity, high birefringence and low confinement losses for liquid analyte sensing applications [J]. Sensors, 2015, 15(12): 31833-31842.
- [9] Asaduzzaman S, Ahmed K, Bhuiyan T, et al. Hybrid photonic crystal fiber in chemical sensing [J]. SpringerPlus, 2016, 5(1): 748-749.
- [10] Sultana J, Islam M S, Faisal M, et al. Highly birefringent elliptical core photonic crystal fiber for terahertz application [J]. Optics Communications, 2018, 407: 92-96.
- [11] Liao K, Liao J F, Xie Y M, et al. A defect photonic crystal fiber with high birefringence and negative dispersion [J]. Laser & Optoelectronics Progress, 2018, 55(7): 070604.
廖昆, 廖健飞, 谢应茂, 等. 一种高双折射负色散的缺陷型光子晶体光纤 [J]. 激光与光电子学进展, 2018, 55(7): 070604.
- [12] Sardar M R, Faisal M. Methane gas sensor based on microstructured highly sensitive hybrid porous core photonic crystal fiber [J]. Journal of Sensor Technology, 2019, 9(1): 12-26.
- [13] Lian Z G, Chen X, Wang X, et al. Preparation and potential applications of microstructured and integrated functional optical fibers [J]. Laser & Optoelectronics Progress, 2019, 56(17): 170615.
廉正刚, 陈翔, 王鑫, 等. 微结构和集成式功能光纤的制备和潜在应用 [J]. 激光与光电子学进展, 2019, 56(17): 170615.
- [14] Cong H F, Li Y C. Single-end inserted homologous methane detector based on hollow-core band gap photonic crystal fibers [J]. Chinese Journal of Lasers, 2020, 47(1): 0111003.
丛海芳, 李彦超. 基于空芯带隙型光子晶体光纤的单

- 端置入式同源甲烷检测仪[J]. 中国激光, 2020, 47(1): 0111003.
- [15] Xie L H, Xu D P, Li M Z, et al. Effects of structural parameters on mode field distribution of photonic crystal fiber[J]. *Laser & Optoelectronics Progress*, 2017, 54(10): 100607.
谢亮华, 许党朋, 李明中, 等. 光子晶体光纤结构参量对模场分布的影响[J]. *激光与光电子学进展*, 2017, 54(10): 100607.
- [16] Liang S J, Zhou C M, Fan D, et al. Experimental study on photonic crystal fiber sensing system based on optical-borne microwave interference[J]. *Laser & Optoelectronics Progress*, 2020, 57(5): 050602.
梁斯靖, 周次明, 范典, 等. 光载微波干涉光子晶体光纤传感系统实验研究[J]. *激光与光电子学进展*, 2020, 57(5): 050602.
- [17] Lu H L, Hu J H. High sensitivity curvature sensor based on SPS fiber structure [J]. *Laser & Optoelectronics Progress*, 2019, 56(8): 080601.
陆杭林, 胡君辉. 基于 SPS 光纤结构的高灵敏度曲率传感器[J]. *激光与光电子学进展*, 2019, 56(8): 080601.
- [18] Xia C M, Zhou G Y. Progress and prospect of microstructured optical fibers [J]. *Laser & Optoelectronics Progress*, 2019, 56(17): 170603.
夏长明, 周桂耀. 微结构光纤的研究进展及展望[J]. *激光与光电子学进展*, 2019, 56(17): 170603.
- [19] Islam M S, Sultana J, Rifat A A, et al. Terahertz sensing in a hollow core photonic crystal fiber[J]. *IEEE Sensors Journal*, 2018, 18(10): 4073-4080.
- [20] Sultana J, Islam M S, Ahmed K, et al. Terahertz detection of alcohol using a photonic crystal fiber sensor[J]. *Applied Optics*, 2018, 57(10): 2426-2433.
- [21] Ebnali-Heidari M, Koohi-Kamali F, Ebnali-Heidari A, et al. Designing tunable microstructure spectroscopic gas sensor using optofluidic hollow-core photonic crystal fiber[J]. *IEEE Journal of Quantum Electronics*, 2014, 50(12): 1-8.
- [22] Dong H Y, Liu C N, Sun S M, et al. Optical fiber high-temperature and refractive index sensor fabricated by femtosecond laser [J]. *Laser & Optoelectronics Progress*, 2019, 56(17): 170633.
董航宇, 刘昌宁, 孙四梅, 等. 飞秒激光制作的光纤高温和折射率传感器[J]. *激光与光电子学进展*, 2019, 56(17): 170633.
- [23] Ma S Z, Feng W L, Peng Z Q, et al. Carbon monoxide gas sensor based on CuO/PANI coated photonic crystal fiber[J]. *Laser & Optoelectronics Progress*, 2019, 56(5): 050603.
马诗章, 冯文林, 彭志清, 等. 基于氧化铜/聚苯胺包覆光子晶体光纤的一氧化碳传感器[J]. *激光与光电子学进展*, 2019, 56(5): 050603.
- [24] Wu Z Q, Shi Z H, Xia H D, et al. Design of highly birefringent and low-loss oligoporous-core THz photonic crystal fiber with single circular air-hole unit [J]. *IEEE Photonics Journal*, 2016, 8(6): 1-11.
- [25] Wu Z Q, Zhou X Y, Xia H D, et al. Low-loss polarization-maintaining THz photonic crystal fiber with a triple-hole core[J]. *Applied Optics*, 2017, 56(8): 2288-2293.
- [26] Sultana J, Islam M S, Atai J, et al. Novel near zero dispersion flattened, low loss porous core waveguide design for terahertz signal transmission[J]. *Optical Engineering*, 2017, 56(7): 074114.

Sensing Characteristics of Near-Infrared Band Based on New Photonic Crystal Fiber

Zhang Wen^{1,2}, Bai Bingbing^{1,2}, Zhang Yanzeng^{1,2}, Chen Cong^{1,2}, Shao Qiyuan^{1,2},
Chen Cancan^{1,2}, Wang Haoran^{1,2}, Liu Hai^{1,2*}

¹ *Engineering Research Center of Ministry of Education for Intelligent Control of Underground Space, China University of Mining and Technology, Xuzhou, Jiangsu 221116, China,*

² *School of Information and Control Engineering, China University of Mining and Technology, Xuzhou, Jiangsu 221116, China*

Abstract

Objective Photonic crystal fibers (PCFs) have wide applications in gas sensing, all-optical switching, four-wave mixing, and other fields due to its unique light control characteristics. In recent years, with the reduction of loss and cost, the sensors based on PCF have the characteristics of short absorption path and sensitive detection, which have become the focus of attention of researchers. However, many scholars have only optimized optical parameters such

as sensitivity and limiting loss, ignoring the influence of the dispersion effect on the optical signal. When the dispersion is too large, it is very likely that the optical pulse will be broadened, causing the overlap of adjacent pulses. Therefore, the increase of the bit error rate will not be conducive to the propagation of light, so it is a challenge to reduce the dispersion and improve the detection sensitivity. Therefore, we have studied the octagonal PCF structure with multi-slot waveguides, which provides the possibility to achieve accurate detection of harmful gases, and at the same time achieves low-dispersion and flat-bandwidth optical signal transmission in the near-infrared wavelength range.

Methods In the infrared spectrum of various gases, the uniqueness of the absorption band is of great significance for the trace amount of the gas. When a beam of light with an intensity of I_0 passes through the photonic crystal fiber, the intensity of light passing through the gas to be measured changes due to the absorption of the light field by the gas to be measured, and the output light intensity I satisfies the Lambert-Beer law. The optimal structure is obtained through parameter optimization, and two grooves close to the core are filled with optical fluid to study the influence of optical fluid technology on optical properties. In order to ensure that the optical fluid only enters the core and not the cladding pores, the optical fluid can be slowly injected into the fiber through a small tip device such as a hypodermic needle or a cladding layer can be deposited on one end of the fiber to block the entry of the optical fluid. With the advent of optical fluids, manipulating light and fluids on a microscopic scale to change the optical capabilities of the medium has become an important means of manufacturing highly sensitive sensors. We adjust the optical characteristics of the photonic circuit through changing the refractive index n , so that the photonic device has tunability and reconfigurability, which can be used for gas sensing detection. In addition, different fluid materials are used to achieve the control of light on substances, and optical fluid technology is introduced into the pores of the optical fiber to dynamically adjust the mode, which reduces the cost caused by replacing the optical fiber and facilitates the construction of a highly sensitive integrated sensor.

Results and Discussions The larger the numerical aperture (NA), the more advantageous it is for sensing applications. When the refractive index difference between the core and the cladding of the PCF is larger, the NA is closer to 1. In this paper, under the best design parameters, we get the NA of 0.11 (Fig. 5), and most of the previously proposed sensor structures ignore this characteristic of PCF. The incident light in the Y polarization direction has higher sensitivity (Fig. 8), so a polarization controller is added between the light source and the sensor to control the light entering the sensor to be linearly polarized light along the Y direction. Since the optical fluid is filled to increase the effective refractive index (A_{eff}), the A_{eff} is significantly moved up compared to the unfilled structure, the NA is decreased, but the change of NA is small compared to the unfilled structure (Fig. 10). In practical applications, it is necessary to consider the dispersion. The dispersion range obtained in the range of $1.55\text{--}1.64\ \mu\text{m}$ is $(0.041 \pm 0.023)\ \text{ps} \cdot \text{THz}^{-1} \cdot \text{cm}^{-2}$ (Fig. 11). Compared to the previously proposed structure (Table 1), the dispersion of the proposed method is very low and the flatness is significantly improved.

Conclusions This paper designs a new type of PCF, uses finite element method to study the optical characteristics in the near infrared range, and analyzes the influence of filling on relative sensitivity, limiting loss, and dispersion parameters of the optimized structure combined with optical fluid technology. The results show that in the wavelength range of $1.55\text{--}1.64\ \mu\text{m}$, it has obvious flat dispersion characteristics close to zero, and the relative sensitivity is above 65%. By filling the optical fluid in a wide near-infrared wavelength range, the optical signal propagation with a low loss of $1.52 \times 10^{-2} - 2.8 \times 10^{-2}\ \text{dB} \cdot \text{m}^{-1}$ and a ultra-low dispersion of $0.018\ \text{ps} \cdot \text{THz}^{-1} \cdot \text{cm}^{-2}$ is realized. In addition, due to the flexibility of the structure, it is expected to be applied to gas sensing detection in the THz range by adjusting the structural parameters.

Key words photonic crystal; relative sensitivity; dispersion; gas detection

OCIS codes 060.5295; 280.4788; 160.5298